Direct Z-scheme polymeric heterojunction boosts photocatalytic hydrogen production via a rebuilt extended π-delocalized network

Linpeng, Xu[a,#], Bining Tian[a,#], Tianyue Wang[a,c,#], Ying Yu[c], Yucheng Wu[a,b,*], Jiewu Cui[b], Zhongnan Cao[b], Jianhong Wu[c], Weike Zhang[a], Qi Zhang[d,*], Jiaqin Liu[d], Zhanfeng Li[c,*] and Yue Tian[a,*]

[a] *Institute of New Carbon Materials, College of Materials Science and Engineering, Taiyuan University of Technology, Taiyuan 030024, China*

[b] *Key Laboratory of Advanced Functional Materials and Devices of Anhui Province & School of Materials Science and Engineering, Hefei University of Technology, Hefei 230009, China*

[c] *Key Laboratory of Advanced Transducers and Intelligent Control System of Ministry of Education, College of Physics and Optoelectronics, Taiyuan University of Technology, Taiyuan 030024, China*

[d] *Institute of Industry & Equipment Technology, Hefei University of Technology, Hefei 230009, China*

[#]These authors contributed equally; [*]Correspondence and requests for materials: tianyue@tyut.edu.cn (Y.T.), wyc@tyut.edu.cn (Y.W.), zhangq@hfut.edu.cn (Q.Z.), and lizhanfeng@tyut.edu.cn (Z.L.)

Materials and Methods

Preparation of T-1ClB-T monomer. All the chemicals were purchased from Aladdin and used without further purification. Thiophene-chlorobenzene-thiophene (T-1ClB-T) monomer was prepared by one-step Stille coupling reaction. In a typical procedure, 1,4-dibromo-2-chlorobenzene (0.89 mmol, 240 mg), tributyl(4-octylthiophen-2-yl)tin (1.95 mmol, 947.9 mg) and 15 mL of toluene were added into a two-neck flask under vigorous stir in nitrogen atmosphere. Until completely dissolved, tetrakis(triphenylphosphine)palladium was added to the reaction mixture, and then stirred at 110 °C for 48 hours. After cooling to room temperature naturally, the reaction mixture was transferred into Milli-Q water and extracted three times with dichloromethane. The organic layer was washed with saturated sodium chloride solution three times and dried with anhydrous MgSO$_4$. After the removal of solvent, the crude product was purified by column chromatography on a silica gel using petroleum ether as the eluent. Colorless T-1ClB-T oily liquid is obtained with a yield of 60.4%.
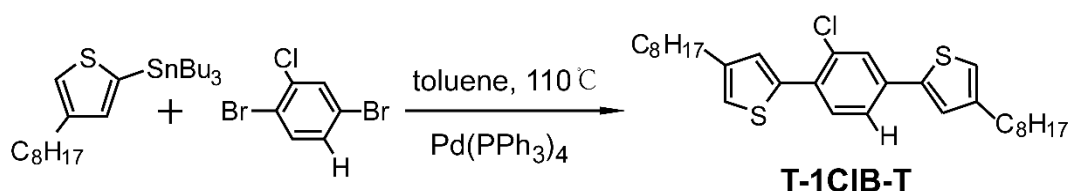
Preparation of Br-T-1ClB-T-Br monomer. 5,5'-(2-chloro-1,4-phenylene)bis(2-bromo-3-octylthiophene) (Br-T-1ClB-T-Br) was prepared by the bromination reaction of T-1ClB-T. Typically, T-1ClB-T (0.427 mmol, 135.4 mg) was dissolved in 20 mL of DMF in a two-neck flask under stirring. The solution was cooled to 0 °C and then NBS (0.59 mmol, 105.1 mg) solution dissolved in DMF was added dropwise to the flask. The reaction mixture was kept at room temperature overnight under stirring. Then, the mixture was transferred into Milli-Q water and extracted with CH$_2$Cl$_2$. Followed by drying with anhydrous MgSO$_4$, the crude compound was purified by silica gel and the solid product was obtained with a yield of 80%.
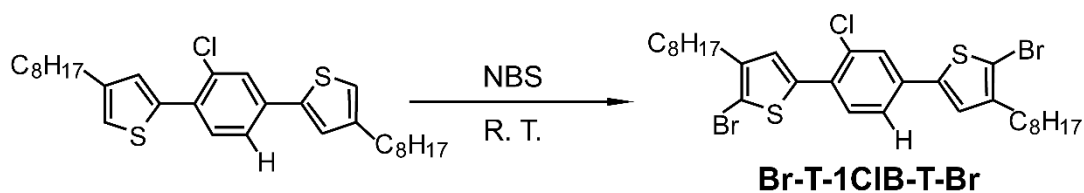
Br-T-1ClB-T-Br

Preparation of P1Cl-T. In a 150 mL three-neck flask, Pd(PPh$_3$)$_4$ (70.5 mg) was added to a solution of distannylated BDT (0.8 mmol, 722.88 mg) and Br-T-1ClB-T-Br (0.96 mmol, 632.39 mg), followed by degassing with nitrogen. The reaction temperature was then raised and kept at 110 °C for 48 hours under continuous stirring. The mixture was then transferred into Milli-Q water and extracted three times with ether. The organic layer was washed and then dried with anhydrous MgSO$_4$ for 6 hours. After the removal of solvent, the crude product was recrystallized using methanol and purified by sorbite extraction. The purified product was transferred to chloroform, followed by recrystallization again with methanol. After drying in vacuum at 70 °C for 8 hours, the product was finally collected with a yield of 53%.
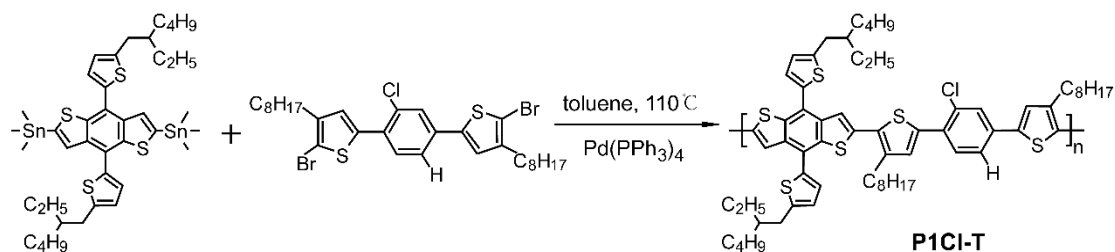
Preparation of g-C$_3$N$_4$. Typically, 10 g of urea was put in a covered crucible and heated with a ramping rate of 10 °C min^{-1} to 550 °C and kept at for 3 h under ambient environment. After cooling down to room temperature naturally, the obtained light-yellow powder was collected without any further treatment.

Preparation of g-C$_3$N$_4$/P1Cl-T. First, a certain mass ratio of the as-prepared g-C$_3$N$_4$ and P1Cl-T were dispersed in 20 mL of chloroform and sonicated for 1.5 h. Followed by vigorous stirring at room temperature for another 5 h, the mixed solution was dried with a gentle argon flow. The product was washed with chloroform and ethanol and spin filtered until the spin throughs were colorless. After being

dried in vacuum at 60 °C, the product was collected for further characterizations. The mass ratios of P1Cl-T to g-C_3N_4 are 3, 5, 7 and 10 wt%, and the resulting samples were labeled as g-C_3N_4/P1Cl-T_3, g-C_3N_4/P1Cl-T_5, g-C_3N_4/P1Cl-T_7, and g-C_3N_4/P1Cl-T_{10}, respectively.

Photocatalytic reaction. Photocatalytic H_2 production activity was measured in a top-irradiation-type Pyrex cylindrical vessel with TEOA as sacrificial agents under the irradiation of Xe lamp equipped with an ultraviolet-cutoff filter ($\lambda \geq 420$ nm). Typically, 2 mg of photocatalyst and 4 μL of chloroplatinic acid aqueous solution (13.3 mg mL^{-1}) were added in 10 mL of aqueous solution containing 2 mL of TEOA as sacrificial reagents in the reaction cell. Before irradiation, the suspension was purged with argon (99.999%) for 20 min to remove any dissolved air. The reactor cell was then irradiated by the Xe lamp ($\lambda \geq 420$ nm, 600 mW cm^{-2}) under magnetic stirring at 15 °C with the assistant of circulating cooling water. The gaseous products were analyzed by a gas chromatograph system (Agilent 8860, TCD detector, Ar carrier gas and 5 Å molecular sieve column) via manual injection with a gas-tight syringe (SGE syringe, TRAJAN, 500 μL).

AQYs measurements. For the AQYs measurements, 15 mg of photocatalyst and 90 μL of chloroplatinic acid aqueous solution (13.3 mg mL^{-1}) were added in 10 mL TEOA aqueous solution in the reaction cell. After degassing by Ar for 20 min, the reaction cell was irradiated for 1 h by Xe light resource equipped with a beam homogenizer and band-pass filter of $\lambda \pm 10$ nm, in which the irradiation area (cover the top with tin foil with 0.5 cm-diameter hole, Fig. S25, ESI) was 0.25 cm^2 and light density was monitored by a digital photodiode power meter (Thorlabs, model PM100D). The AQYs were calculated as follows[1].

$$\text{AQY}(\%) = \frac{Number\ of\ reacted\ electrons}{Number\ of\ incident\ photons} \times 100\%$$
$$= \frac{Number\ of\ evolved\ hydrogen\ molecules \times 2}{Number\ of\ incident\ photons} \times 100\%$$

Photocatalyst characterization. The ^1H NMR spectra of the intermediate product was recorded on a

Bruker Fourier 400 M spectrometer, where $CDCl_3$ was used as solvent. The molecular weight of P1Cl-T

is measured by Waters 1515 gel permeation chromatography, in which the mobile phase is

tetrahydrofuran, and the standard product is polystyrene, respectively. XRD patterns were recorded on

a SHIMADZU XRD-6100 powder diffractometer using Cu-Kα radiation (λ = 0.15406 nm). The morphology

and microstructure were inspected by field emission scanning electron microscope (SU8010, Hitachi).

TEM, HRTEM and HAADF-STEM and STEM-EDX mapping were collected with a Tecnai G2 F30 electron

microscope at an acceleration voltage of 300kV. STEM-EELS measurements were performed on JEM-

ARM200F TEM with probe spherical aberration corrector. ESCALAB-250 XPS spectrometer system with

Al Kα source was utilized to determine the chemical states and the valence band spectra. All the binding

energies were referenced to the C 1s peak at 284.8 eV of the surface adventitious carbon. Absorbance

measurements were performed using an Agilent Cary 5000 ultraviolet-visible-infrared

spectrophotometer with $BaSO_4$ as the reflectance standard. FTIR spectra are measured by Thermo

Nicolet 360 IR spectrophotometer in the range 400-4000 cm^{-1}, where the detector was cooled by liquid

nitrogen before measurements. The samples were prepared in KBr pellets for the spectral

measurements. The steady-state fluorescence spectra and time-resolved transient fluorescence spectra

of all samples were obtained by the Edinburgh FLS 1000 fluorescence spectrometer. TA measurements

were carried out on a regenerative amplified Ti: sapphire laser system from coherent corporation (800

nm, 35 fs, 6 mJ/pulse, and 1 kHz repetition rate) in combination with nonlinear frequency mixing

techniques and the ultrafast Helios spectrometer. Part of the 800 nm output pulse from the amplifier

was used to pump a TOPAS Optical Parametric Amplifier (OPA) which generates the 365 nm pump beam.

The pump pulses were chopped by a synchronized chopper at 500 Hz and the absorbance change was

calculated with two adjacent probe pulses (pump-blocked and pump-unblocked), and the pump energy

was approximately 1.5 μJ. During the measurements, samples were dispersed in a quartz cuvette with stirring. KPFM measurements were carried out on an atomic force microscopy (AFM, Bruker) equipped with an irradiation system (Park system, NX10) to analyze the morphology and surface potential.

Electrochemical measurement. Energy band structures of PxCl-T (x = 0, 1 and 2) and g-C_3N_4 were determined by cyclic voltammetry on Versa STAT3 electrochemical workstation using a three-electrode system of glassy carbon electrode as working electrode, platinum electrode as counter electrode and Ag/AgCl as reference electrode, respectively. Typically, the sample was dissolved in chloroform to yield a concentration of 0.5 mg mL^{-1} and then drop casted onto the glassy carbon electrode. Three electrodes were placed in an electrolyte of 0.1 M tetrabutylammonium perchlorate in acetonitrile solution. Before measurements, the oxidation peak of the water was removed by N_2 degassing for 2 min. Using ferrocene/ferrocenium (Fc/Fc$^+$) redox potential as the internal standard, the HOMO and LUMO energy levels of the samples can be determined by[2].

$$E_{HOMO} = -e\left(E_{ox\_onset} - E_{ox}(ferrocene) + 4.81\right)(eV)$$

$$E_{LUMO} = E_{HOMO} + E_g$$

The Mott-Schottky (M-S) curves were measured by a conventional three-electrode system consisting of ITO glass as working electrode, platinum electrode as counter electrode, Ag/AgCl as reference electrode and 0.5 M H_2SO_4 as electrolyte[3]. For the preparation of the working electrode, typically, 5 mg of samples were dispersed in a mixed solution containing 250 μL of Milli-Q water and 250 μL of ethanol. Then 30 μL of naphthol was added and ultrasonication was performed for 30 min. 106 μL of the dispersed solution was drop casted onto ITO glass as the working electrode (1 mg cm^{-2}). The photocurrent density-time curves (bias: 0.5 V) and EIS were tested in the same way as M-S, except that the electrolyte was replaced with 0.5 M Na_2SO_4 and xenon lamp was used as the light source.

DFT calculations. The density functional theory (DFT) calculations were performed with the Vienna Ab initio Simulation Package (VASP 5.4) based on projector augmented wave (PAW) method[4, 5]. PerdewBurke-Ernzerhof (PBE) functional within generalized gradient approximation is adopted to treat electronic exchange-correlation energy[6]. Grimme's semi empirical dispersion corrected DFT-D3 method was used to describe Van der Waals (vdW) interaction[7]. The plane-wave cutoff energy is set to 400 eV. The convergence criteria for structural optimization are set as 0.1E-05 eV and 0.03 eV A^{-1} for energy and force, respectively. The vacuum layer of 20 Å is used to avoid interaction between adjacent layers. For the charge density difference, the monomers that can represent its structural characteristics were used for of $g\text{-}C_3N_4$ and polymer. For the Gibbs free energy calculation, integration in Brillouin zone is performed to optimize geometric configuration using the k-point mesh of 3×3×3 on the basis of the Monkhorst-Pack scheme for $g\text{-}C_3N_4$, P1Cl-T and $g\text{-}C_3N_4$/P1Cl-T[8]. The Gibbs free energy ΔG_{H*} can be calculated as follows: $\Delta G_{H*} = \Delta E_{H*} + \Delta E_{ZPE} - T\Delta S_{H*}$. ΔE_{H*} is the adsorption energy of the H atom. ΔE_{ZPE} is the difference in the zero-point energy of hydrogen in the adsorbed state and the gas phase. The entropy difference is denoted as ΔS_{H*}. T is the room temperature, and ΔS_{H*} is considered as half the entropy of H_2 in the gas phase under standard conditions. The frontier molecular orbital calculations were carried out with the Gaussian 09 program[9]. The B3LYP[10, 11]/GEN method (GEN1:6-31g* for C, H, N, S and LANL2DZ for Cl) were used for geometry optimization. For better description of the weak interaction, the Grimme-D3 correction is added for the hybrid structure.
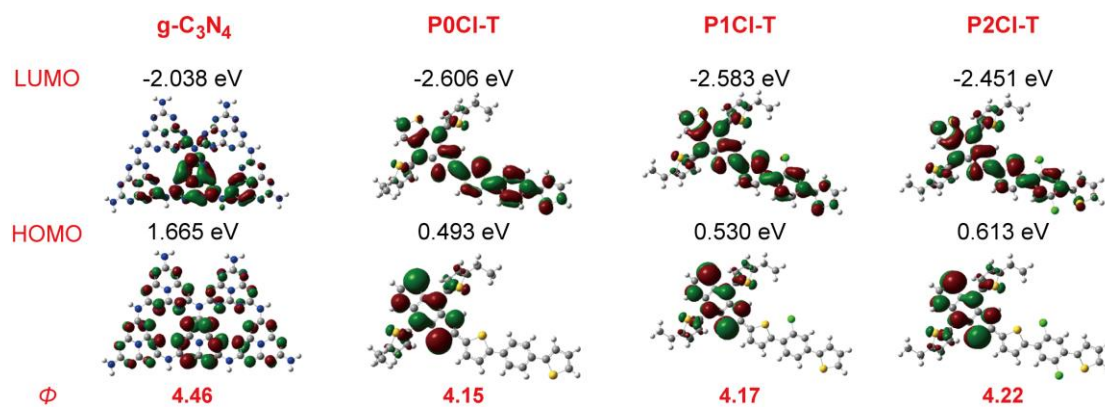
Fig. S1. The calculated frontier molecular orbital levels of g-C$_3$N$_4$ and PxCl-T (x = 0, 1, and 2).

The LUMO energy levels for polymers PxCl-T (x = 0, 1 and 2) are -2.606, -2.583 and -2.451 eV, while the HOMO energy levels are 0.493, 0.530 and 0.613 eV, respectively. Both LUMO and HOMO levels exhibit downshift with the increase of Cl substitution. The work functions of PxCl-T are 4.15, 4.17 and 4.22 eV, respectively, which are smaller than that of g-C$_3$N$_4$ (4.46 eV), suggesting the lower lying E$_f$ of g-C$_3$N$_4$ compared to that of PxCl-T.
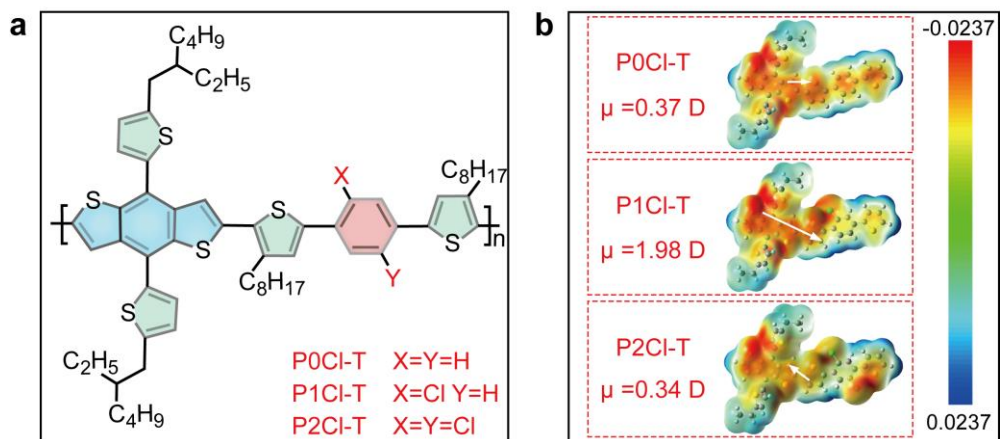
Fig. S2. a, Chemical structures of PxCl-T (x = 0, 1, and 2). b, Electrostatic potentials distribution for PxCl-T (x = 0, 1, and 2).
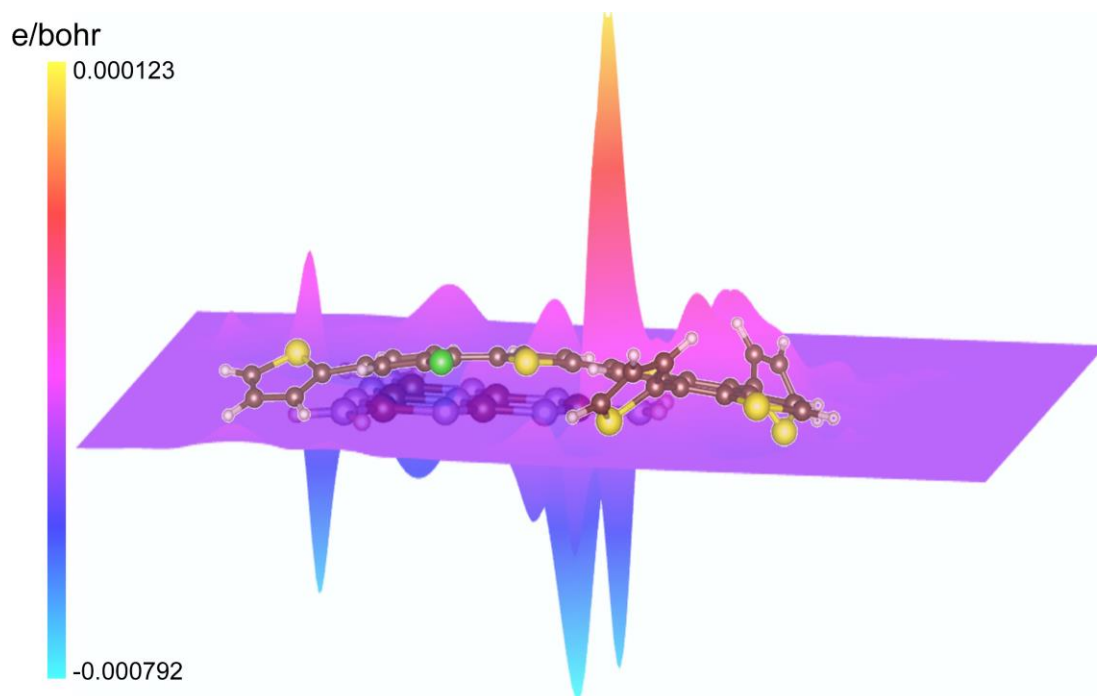
Fig. S3. 2D data display of the charge density difference for the slice of the g-C_3N_4/P1Cl-T polymeric heterojunction. It shows obvious charge accumulation and depletion peaks, further confirming the charge transfer at the interface.
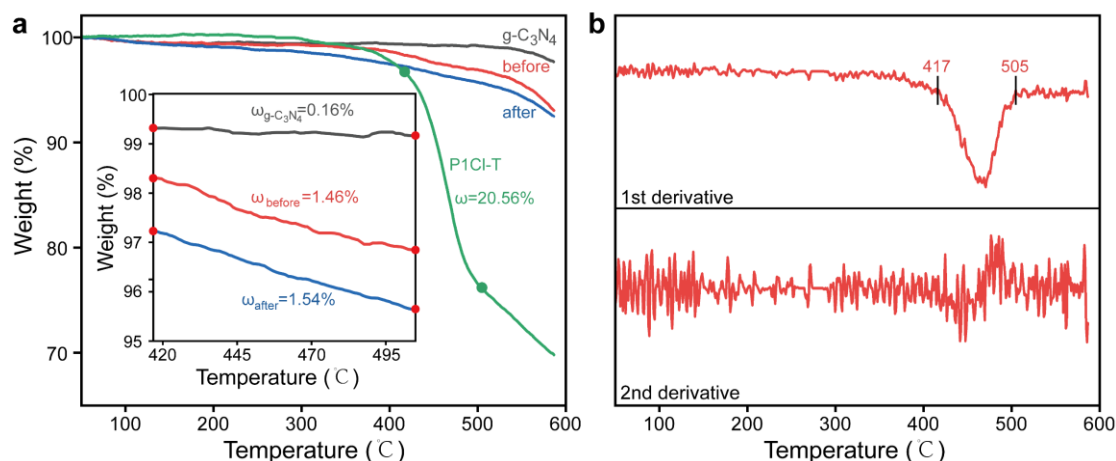
Fig. S4. Analysis of P1Cl-T mass ratio in g-C_3N_4/P1Cl-T_7 photocatalyst. a, TGA curves of the P1Cl-T, g-C_3N_4 and g-C_3N_4/P1Cl-T_7. Legends "before" and "after" represent pristine and recovered g-C_3N_4/P1Cl-T_7 samples from photocatalytic reactions, respectively. b, Differential TGA curve of P1Cl-T in a.

As shown in the range of 417-505 °C, there is almost no mass change of g-C_3N_4, where P1Cl-T decomposes quickly. Therefore, we used the mass change in this temperature range to determine the mass percentage of P1Cl-T in g-C_3N_4/P1Cl-T_7 photocatalyst based on the following equation:

$$w = \frac{\left(\omega_{417\sim505} - \omega_{g-C_3N_4}\right)}{\omega_{P1Cl-T}} * 100\% \cdots\cdots\cdots\cdots\cdots Eq.\,(1)$$

In the equation (1), w represents the mass percentage of P1Cl-T in g-C_3N_4/P1Cl-T_7; $\omega_{417\sim505}$, $\omega_{g-C_3N_4}$ and ω_{P1Cl-T} stand for the mass percentage changes of g-C_3N_4/P1Cl-T_7 before or after photocatalysis, g-C_3N_4 and P1Cl-T in the temperature range of 417-505 °C, respectively. According to Eq. (1), the mass percentage of P1Cl-T in g-C_3N_4/P1Cl-T_7 before and after photocatalysis is estimated to be ca. 6.33 % and 6.71%, respectively. Based on the existence of experimental and measurement errors, we believe that the mass percentage of P1Cl-T in the system before and after photocatalytic reaction changed very little.
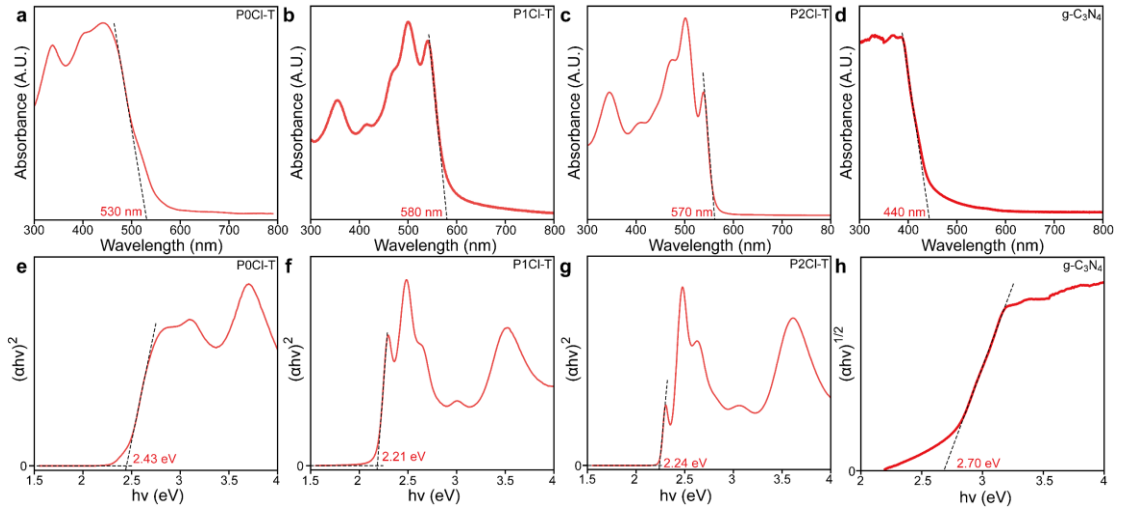
Fig. S5. UV-vis absorption spectra and optical band gap of PxCl-T (x = 0, 1, and 2) and g-C_3N_4. a-d, UV-vis absorption spectra. e-h, the corresponding Kubelka-Munk plots.
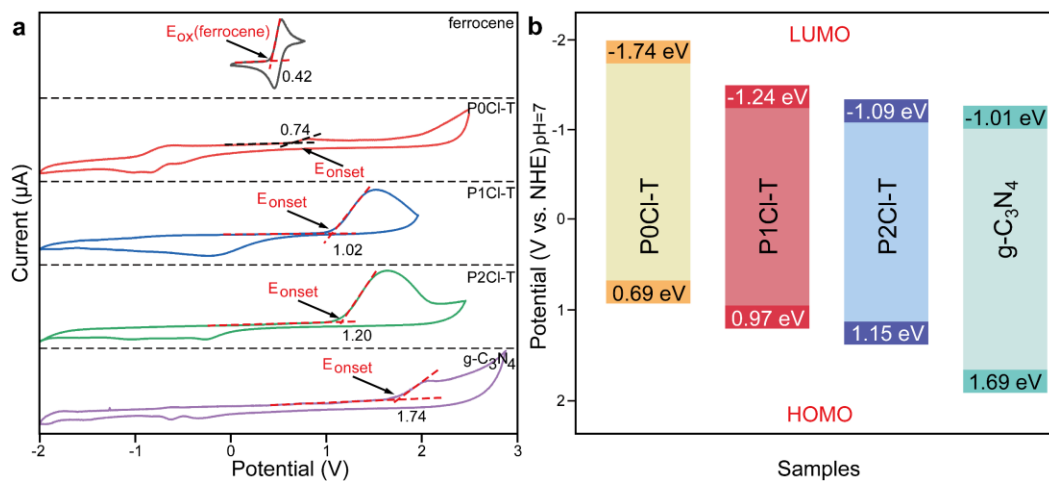
Fig. S6. Energy band structures for PxCl-T (x = 0, 1, and 2) and g-C$_3$N$_4$. a, Cyclic voltammogram of g-C$_3$N$_4$ and PxCl-T (*x* = 0, 1, and 2) on glassy carbon electrode in 0.1 M tetrabutylammonium perchlorate acetonitrile solution at a scan rate of 50 mV s^{-1}. Platinum electrode and Ag/AgCl were used as counter and reference electrodes, respectively. The ferrocene was provided as the internal reference. b, Band structure diagrams for g-C$_3$N$_4$ and PxCl-T (*x* = 0, 1, and 2).
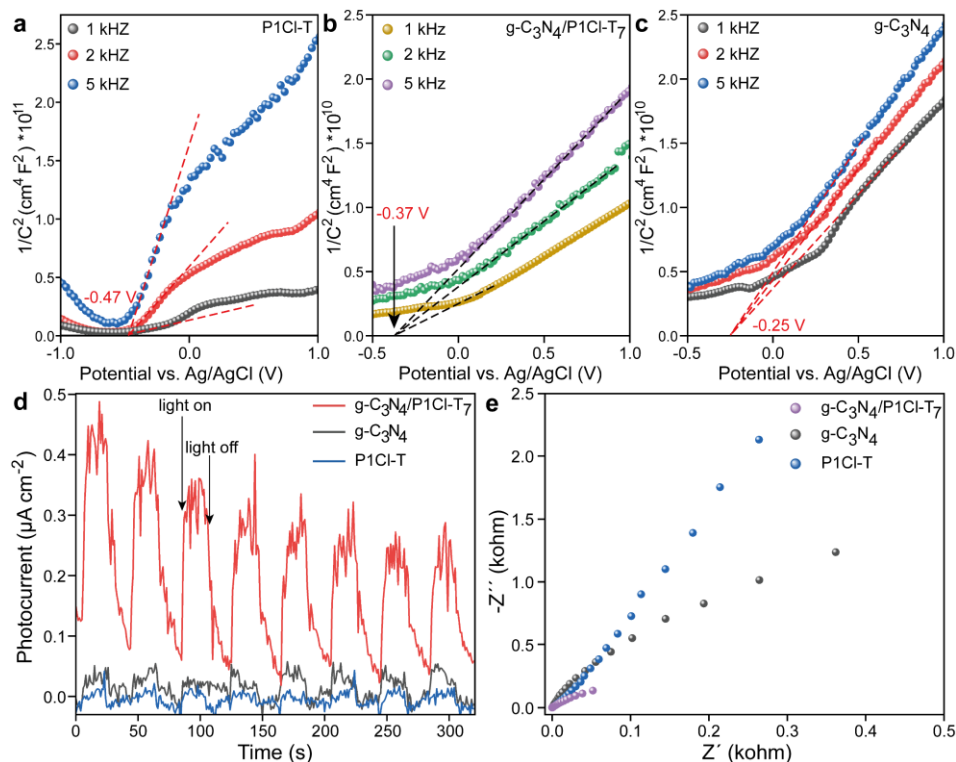
Fig. S7. Photoelectrochemical characterizations of g-C$_3$N$_4$, P1Cl-T and g-C$_3$N$_4$/P1Cl-T$_7$. a-c, M-S plots. d, Photocurrent response. e, EIS.

The M-S plots show positive slope, implying n-type nature of both P1Cl-T and g-C$_3$N$_4$ (Supplementary Fig S7a-c). The flat band potentials (E$_{FB}$) of P1Cl-T and g-C$_3$N$_4$ were determined to be around -0.27 V and -0.05 V (NHE, pH=0), respectively. For n-type semiconductors, E$_{FB}$ can be roughly considered as the Fermi level (E$_f$) [3,12,13]. Therefore, based on the Nernstian function with slope of -59 mV/pH, when pH=7, the Fermi levels of P1Cl-T and g-C$_3$N$_4$ are -0.68 and -0.46 V, respectively. When P1Cl-T and g-C$_3$N$_4$ was assembled to form g-C$_3$N$_4$/P1Cl-T heterojunction, the E$_f$ of P1Cl-T and g-C$_3$N$_4$ bend and are finally located at the same potential, which can be determined to be around -0.58 V (NHE, pH=7). Furthermore, the photocurrent density was examined to study the charge carrier separation efficiency in g-C$_3$N$_4$/P1Cl-T$_7$. For both P1Cl-T and g-C$_3$N$_4$, the photocurrent densities are very low at a bias voltage of 0.5 V vs Ag/AgCl (Supplementary Fig S7d). When the heterojunction is formed, the photocurrent density of g-C$_3$N$_4$/P1Cl-T$_7$ is significantly increased (ca. 240 nA cm^{-2}), which is attributed to improved charge carrier separation[12]. Supplementary Fig. S7e shows the electrochemical impedance spectroscopy (EIS). As compared, the diameter of the Nyquist circle of g-C$_3$N$_4$/P1Cl-T$_7$ is significantly smaller than that of pure P1Cl-T and g-C$_3$N$_4$, suggesting that the formation of g-C$_3$N$_4$/P1Cl-T$_7$ heterojunction can decrease the interfacial charge transfer resistance, which is in favor of photogenerated carriers transfer and separation, and finally boosts the HER performance.
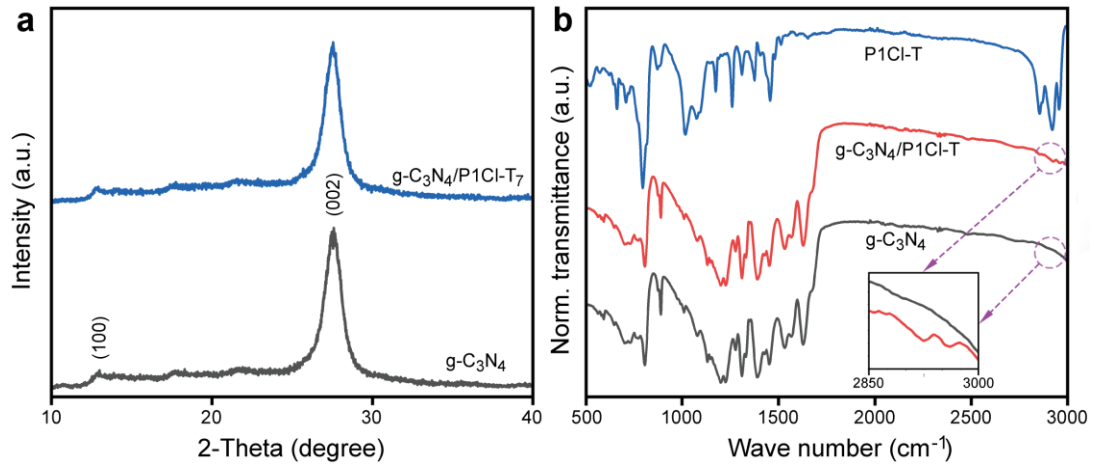
S14

Fig. S8. a, XRD patterns of g-C_3N_4 and g-C_3N_4/P1Cl-T_7. b, FTIR spectra of g-C_3N_4, P1Cl-T and g-C_3N_4/P1Cl-T_7. The inset is zoom of the FTIR spectra in the range of 2850-3000 cm^{-1}.
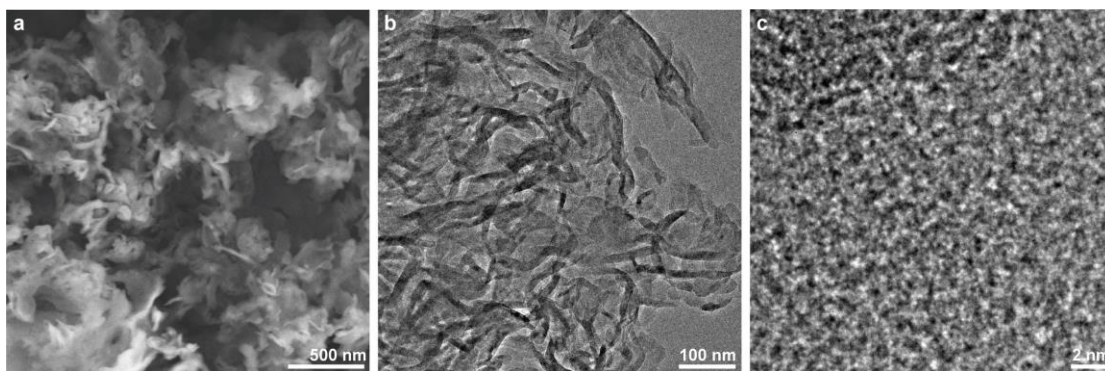
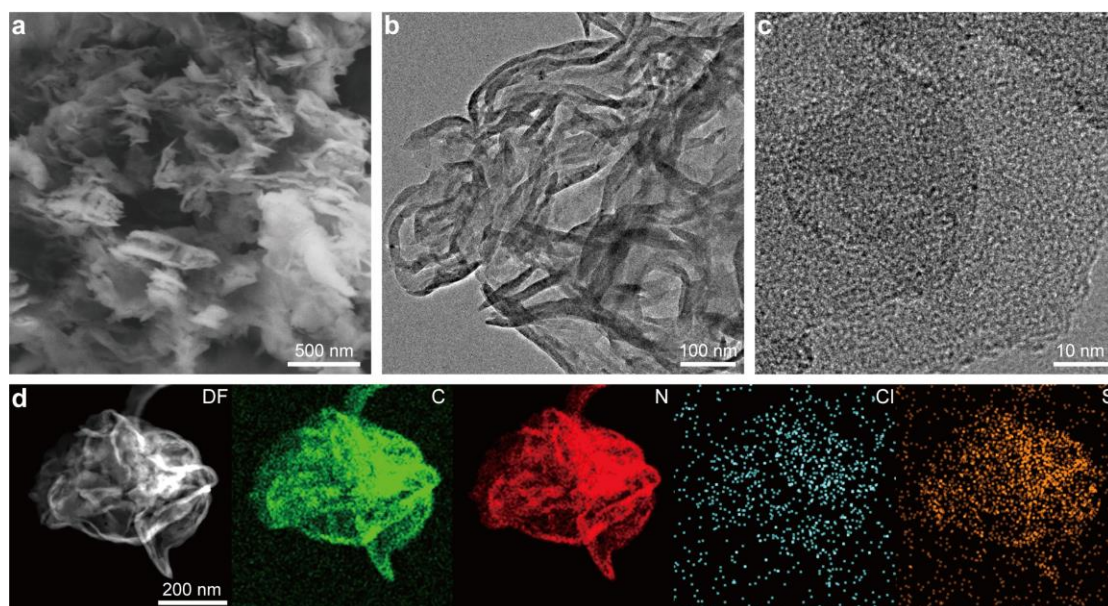Fig. S9. Microstructure of pristine g-C$_3$N$_4$. a, SEM image. b, TEM image. c, HRTEM image.

Fig. S10. Microstructure of pristine g-C$_3$N$_4$/P1Cl-T$_7$. a, SEM image. b, TEM image. c, HRTEM image. d, EDS elemental mapping.
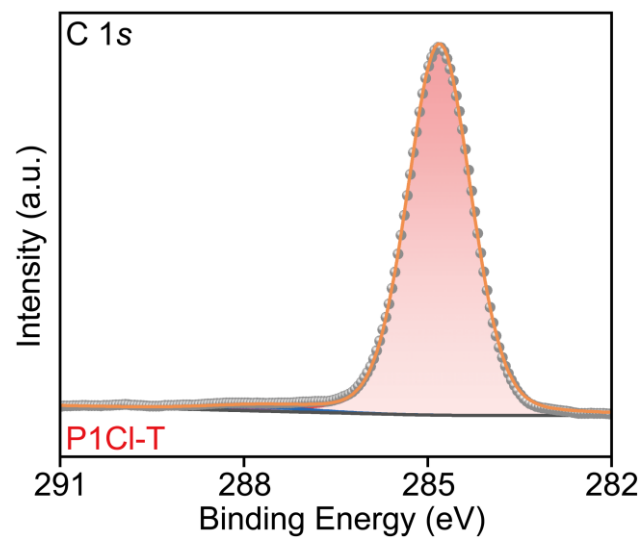
Fig. S11. C 1*s* XPS fine spectrum of P1Cl-T.

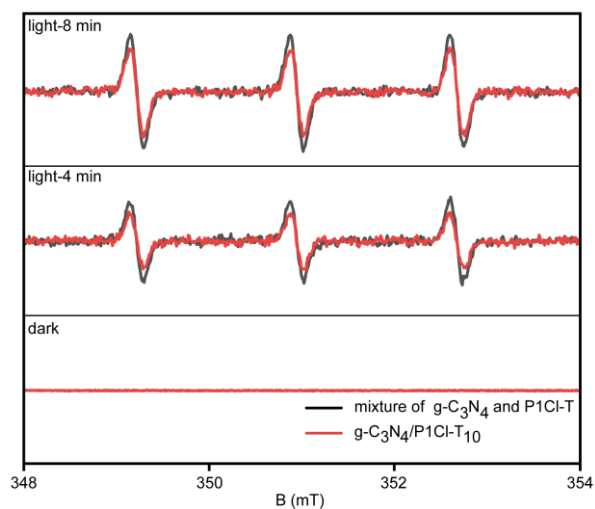Fig. S12. ESR signals of singlet oxygen ($^1O_2$) for g-C_3N_4/P1Cl-T_{10} heterostructure and physical mixture of g-C_3N_4 and P1Cl-T under light irradiation.

Compared with the physical mixture of P1Cl-T and g-C_3N_4, the singlet oxygen signal intensity of g-C_3N_4/P1Cl-T_{10} heterostructure is reduced, indicating that the π-π stacking between P1Cl-T and g-C_3N_4 leads to the quenching of the aggregation-induced excitation energy. In addition, this also shows that the face-to-face arrangement between P1Cl-T and g-C_3N_4 is in favor of proper interface matching, further promoting electron transfer at the interface[14].
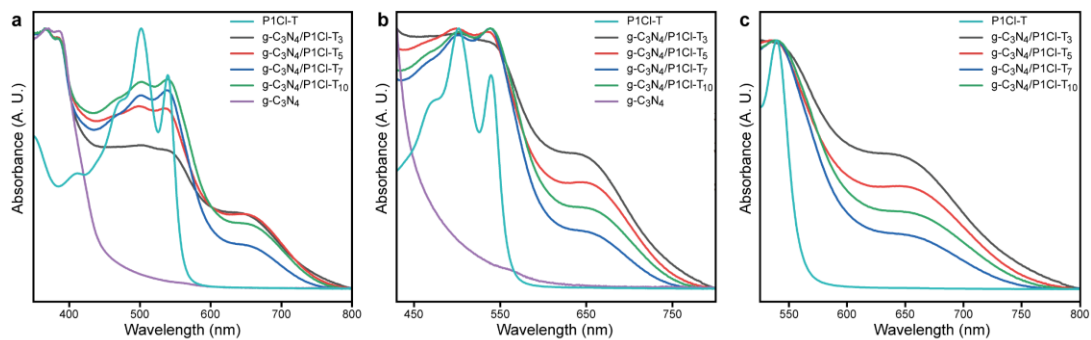
Fig. S13. Absorption spectra of g-C$_3$N$_4$/P1Cl-T with different P1Cl-T content. A, Normalized absorption spectra at 365 nm. b, Normalized absorption spectra at 501 nm. c, Normalized absorption spectra at 539 nm.
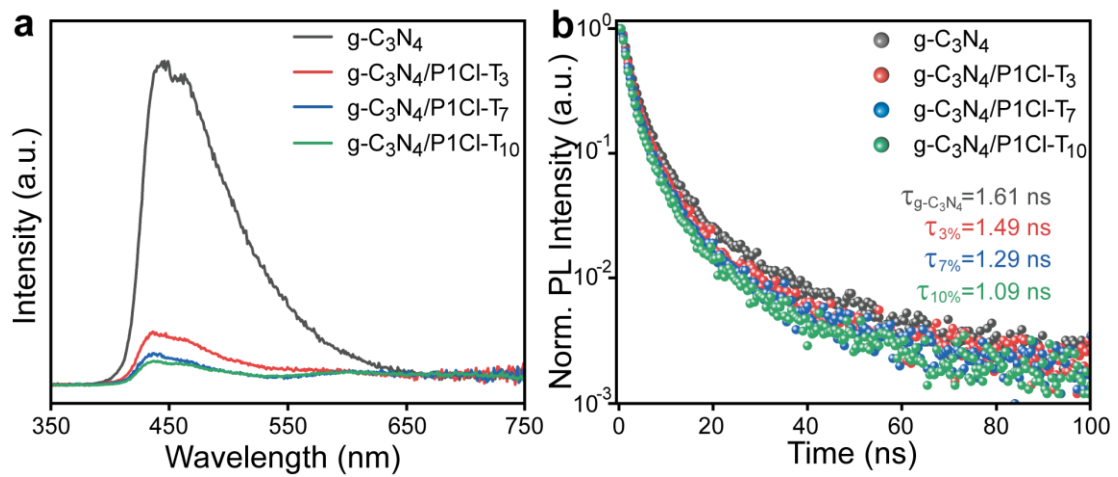
Fig. S14. PL characterizations of g-C$_3$N$_4$/P1Cl-T. a, Steady-state luminescence spectra of g-C$_3$N$_4$/P1Cl-T with different composition ratios. b, Time-resolved PL decay at 437 nm upon 300 nm excitation.
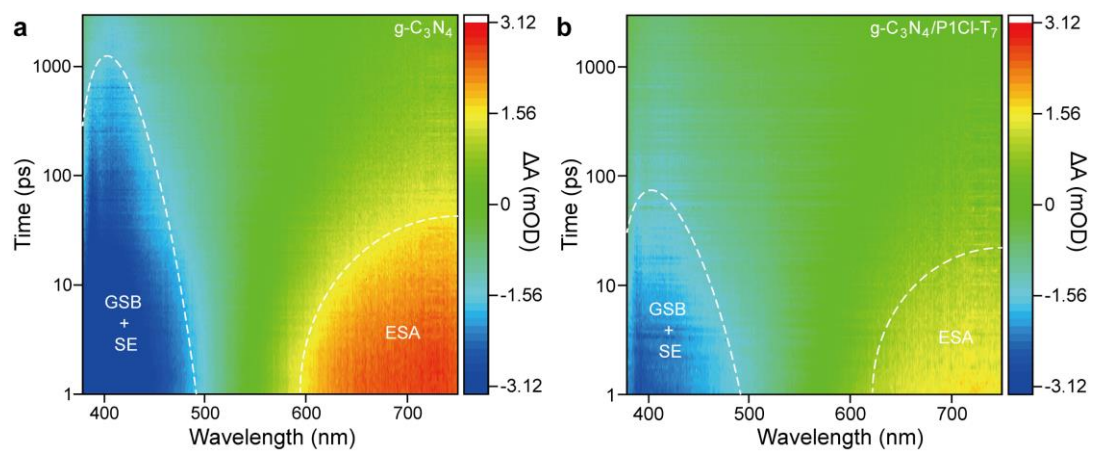
Fig. S15. TA characterizations of g-C$_3$N$_4$ (a) and g-C$_3$N$_4$/P1Cl-T$_7$ (b). The samples were dispersed in chloroform for measurements (pump laser: 365 nm).
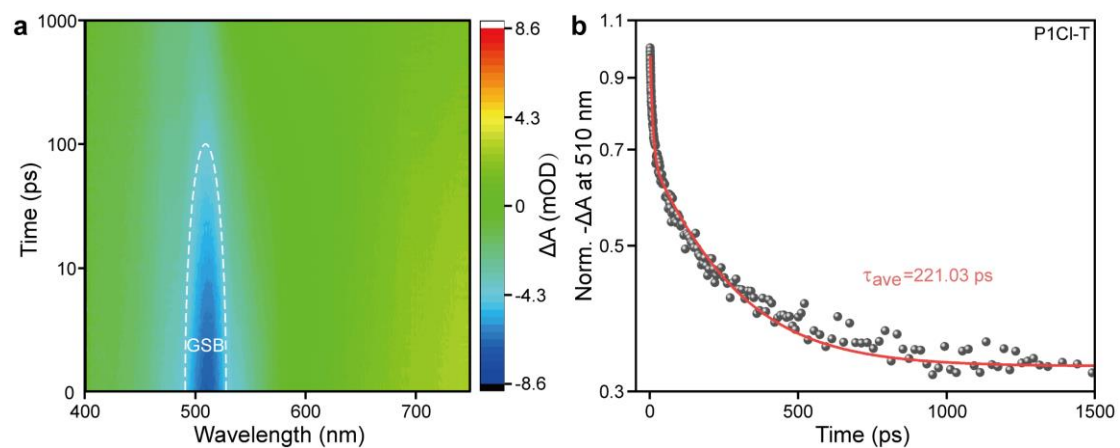
Fig. S16. TA kinetic characterization of P1Cl-T. a, 3D contour plots of fs-TAS observation. b, fs-TA recovery kinetics at 510 nm and the corresponding exponential fitting result. The sample was dispersed in chloroform for measurements (pump laser: 365 nm).
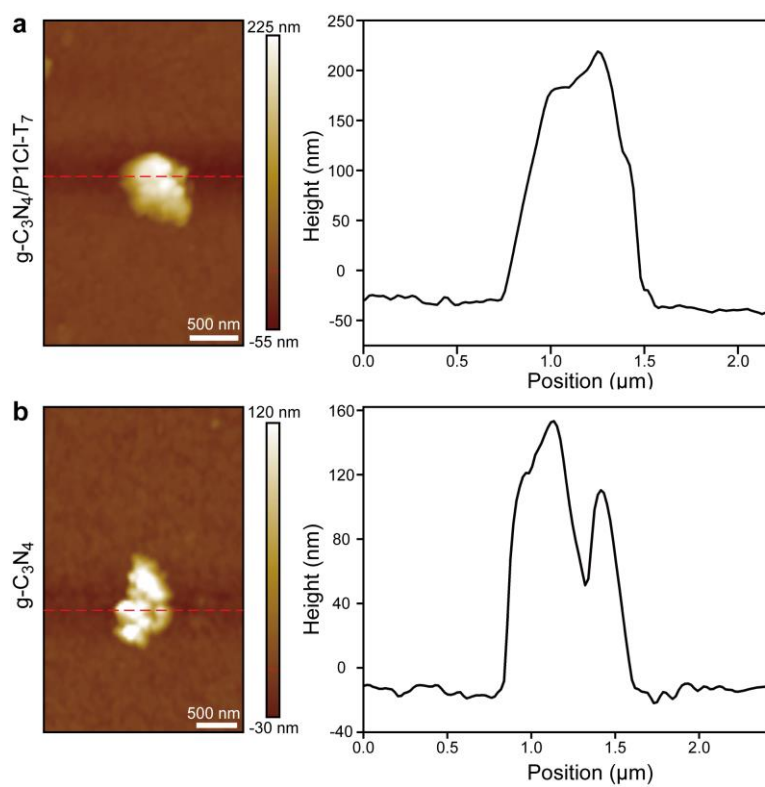
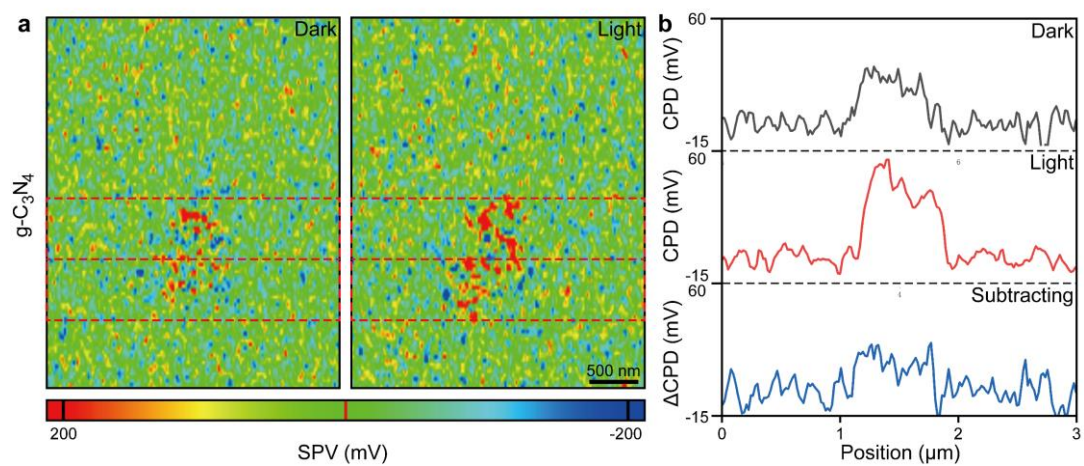Fig. S17. AFM images and the corresponding line profile. a, g-C$_3$N$_4$/P1Cl-T$_7$. b, g-C$_3$N$_4$.

Fig. S18. a, KPFM images of g-C$_3$N$_4$ in the dark (left) and upon ≥ 420 nm illumination (right). b, Contact potential difference (CPD) profiles of dark state (black line) and light state (red line) across the g-C$_3$N$_4$ and the corresponding SPV profile.
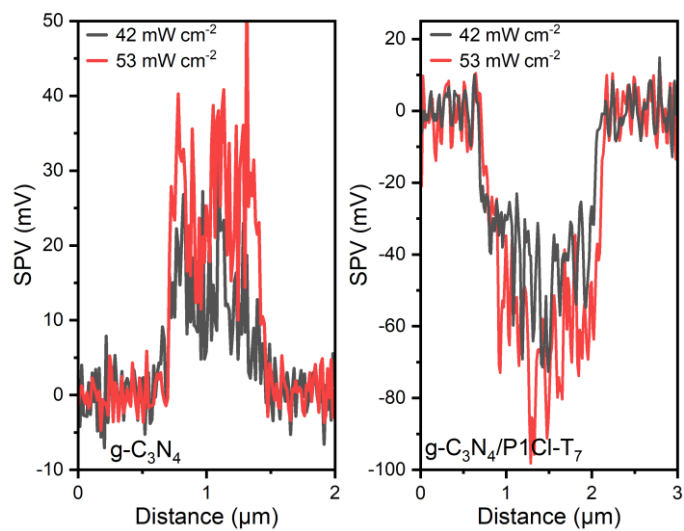
Fig. S19. Surface photovoltage of g-C$_3$N$_4$ (left) and g-C$_3$N$_4$/P1Cl-T$_7$ (right) under illumination at different light intensities.

Fig. S20. Photoelectron kinetic analysis of g-C$_3$N$_4$/P1Cl-T. Absorption and PL spectra of g-C$_3$N$_4$ and P1Cl-T were plotted together with normalized TA spectra of g-C$_3$N$_4$, g-C$_3$N$_4$/P1Cl-T$_7$ in the same time window.
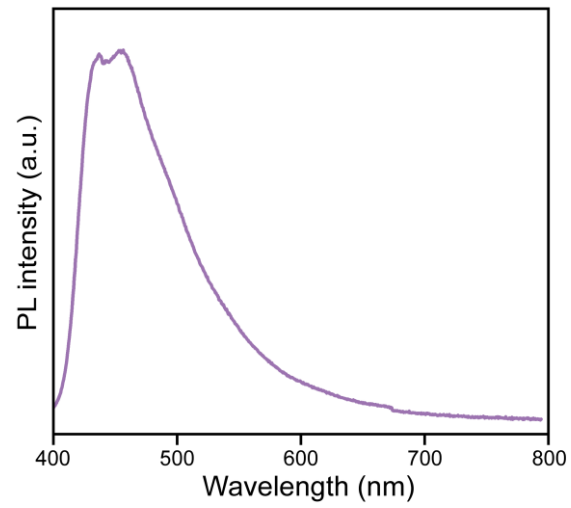
Fig. S21. PL emission spectrum of direct mixed g-C$_3$N$_4$-10*wt*%P1Cl-T under the excitation of 300 nm.

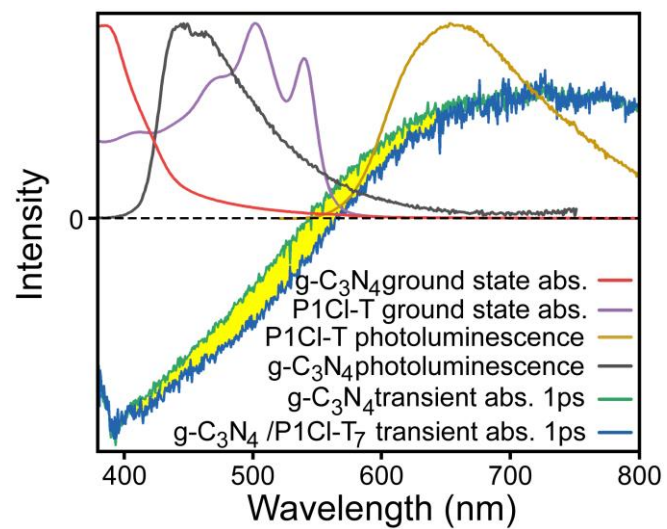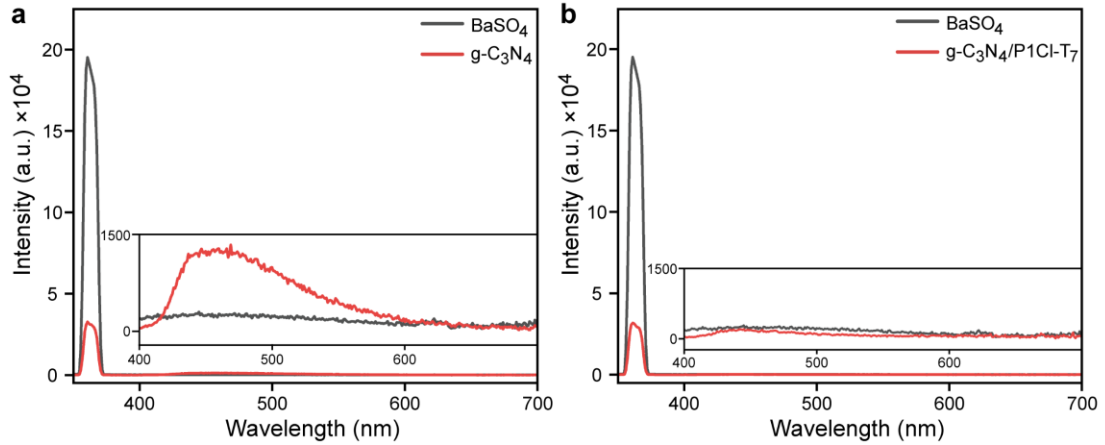Fig. S22. PL emission quantum yield measurements. a, g-C_3N_4. b, g-C_3N_4/P1Cl-T_7. Excitation wavelength is 365 nm and $BaSO_4$ was used as reference.

The PL emission quantum yield can be calculated based on the Eq. (2)

$$\eta = \frac{\int L_S}{\int E_R - \int E_S} * 100\% \cdots\cdots\cdots\cdots Eq.\,(2)$$

where L_S is the emission spectrum of the sample; and E_S and E_R are the excitation light with and without the sample in the integrating sphere, respectively. The PL emission quantum yields for g-C_3N_4 and g-C_3N_4/P1Cl-T are calculated to be 7.8 and 0.76 %, respectively.
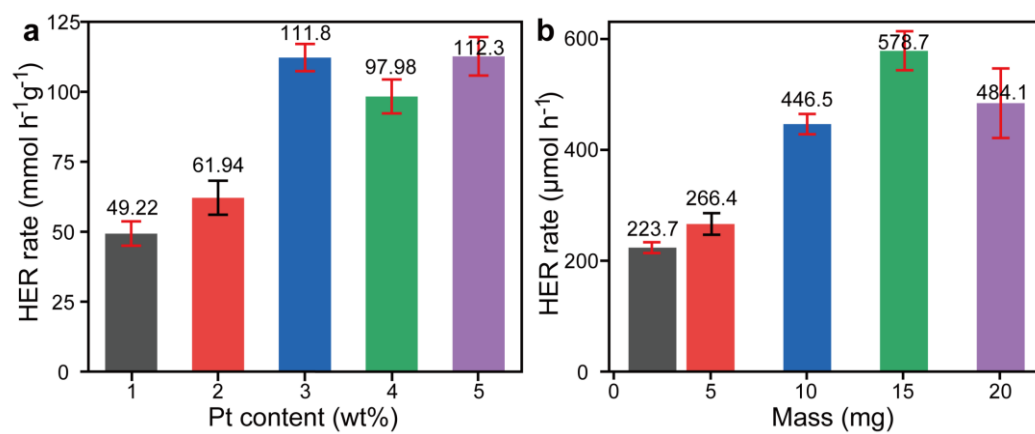
Fig. S23. Photocatalytic H₂ production measurements. a, HER activities as a function of Pt loading amount. b, HER activities as a function of photocatalyst dose. Error bars in a and b were calculated as a percentage uncertainty on the basis of three repeat measurements.
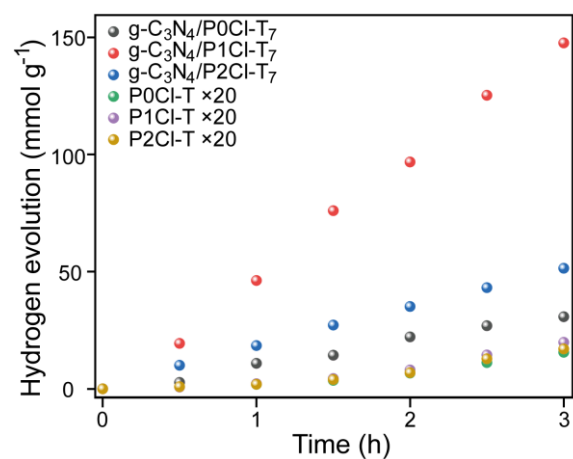
Fig. S24. Time course for photocatalytic H_2 production performance over PxCl-T and g-C_3N_4/PxCl-T_7 (x = 0, 1, and 2) under λ ≥420 nm irradiation. For a better plot, the photocatalytic activities of PxCl-T were enlarged by 20-fold.
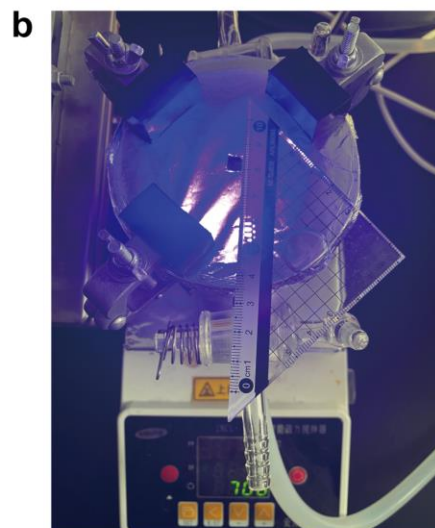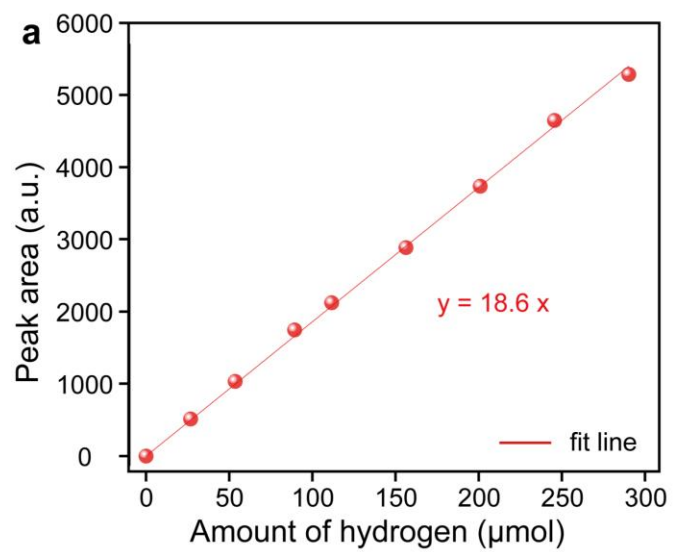
Fig. S25. a, Gas chromatography calibration curve. b, Light spot with the area of 0.25 cm^2 for AQY measurements.
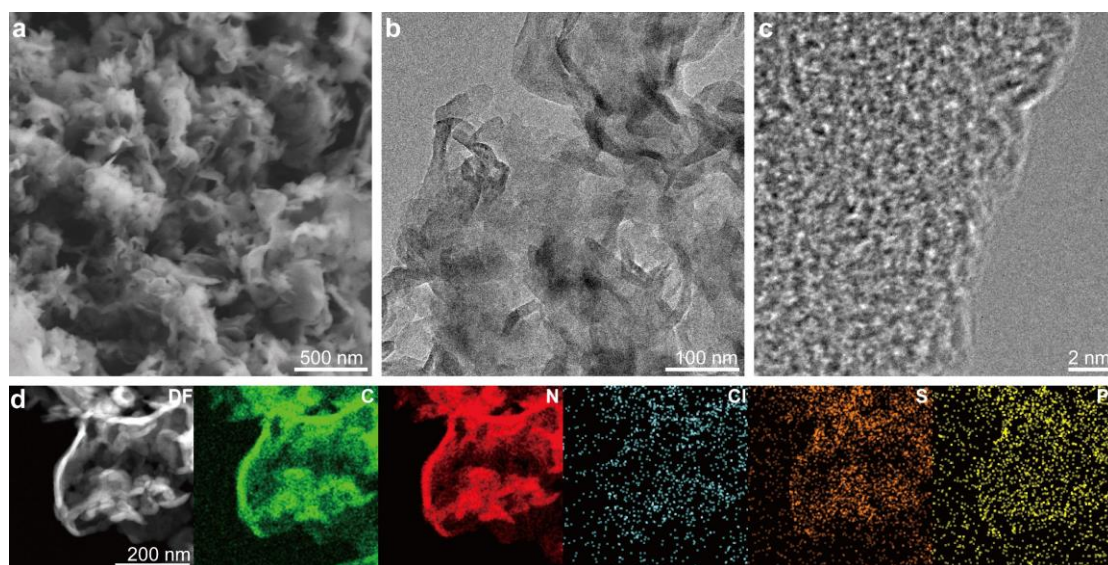
Fig. S26. Microstructure and element distribution map of g-C$_3$N$_4$/P1Cl-T$_7$ recovered after photocatalytic reaction. a, SEM image. b, TEM image. c, HRTEM image. d, EDS elemental mapping.
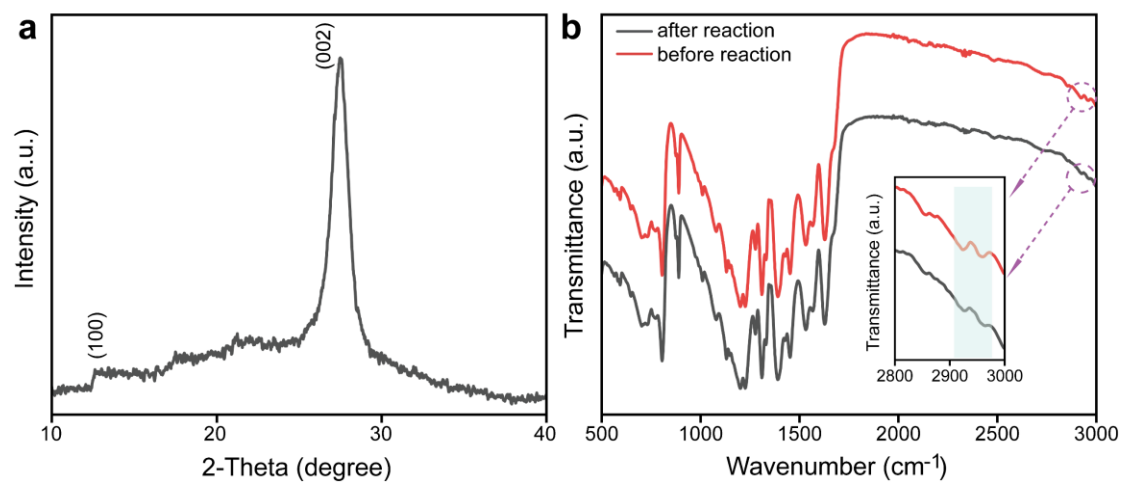
Fig. S27. Structural properties of the recovered g-C_3N_4/P1Cl-T_7 after reaction. a, XRD pattern. b, FTIR spectra. The inset is zoom of the FTIR spectra in the range of 2800-3000 cm^{-1}.
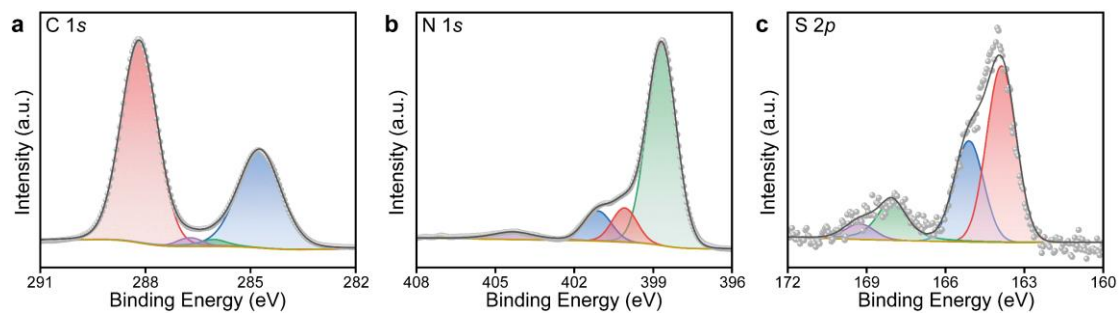
Fig. S28. XPS characterizations of g-C$_3$N$_4$/P1Cl-T$_7$ heterojunction recovered from photocatalytic reaction. a, C 1s. b, N 1s. c, S 2p.
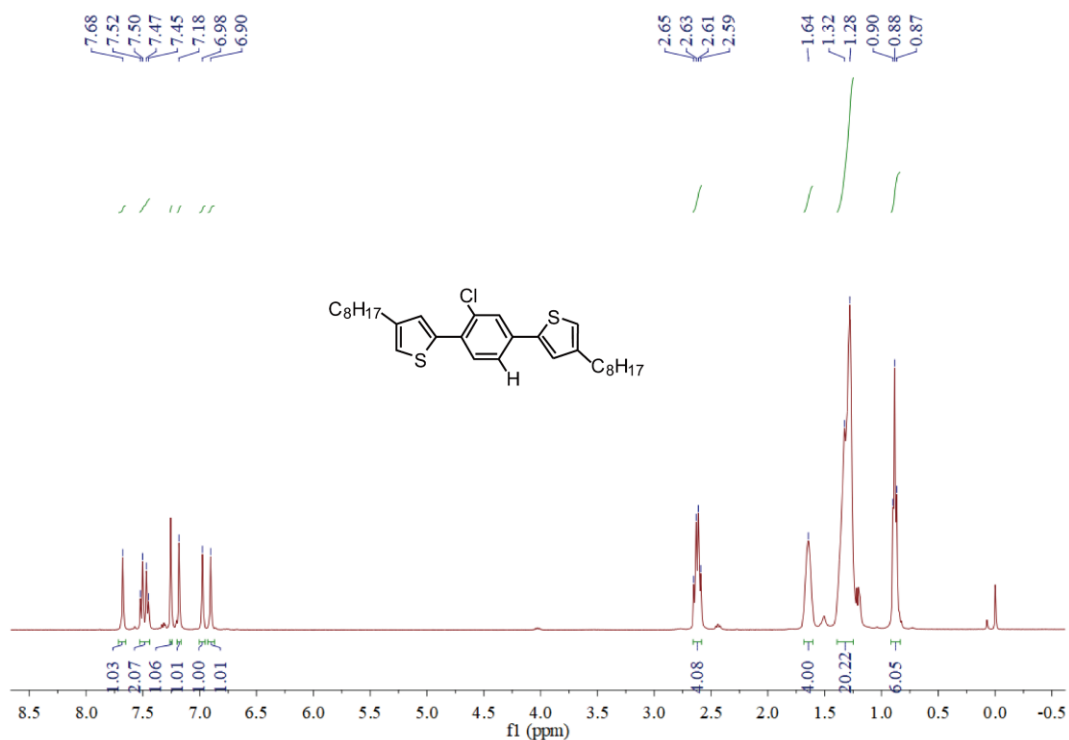
Fig. S29. ^{1}H NMR spectrum of T-1ClB-T. Chemical shifts were recorded in delta (δ) units, expressed in parts per million (ppm). Protonated CDCl$_3$ was used as the solvent for recording ^{1}H (of residual proton; CDCl$_3$, δ = 7.26 ppm). The splitting patterns of ^{1}H NMR have been described as "s, singlet, d, doublet and m, multiple". 1H NMR (400 MHz, CDCl$_3$): δ = 7.68 (s, 1H), 7.49 (dd, J = 21.0, 8.1 Hz, 2H), 7.26 (s, 1H), 7.18 (s, 1H), 6.98 (s, 1H), 6.90 (s, 1H), 2.69-2.53 (m, 5H), 1.64 (s, 5H), 1.28-1.32 (m, 21H) and 0.87-0.90 (m, 7H).
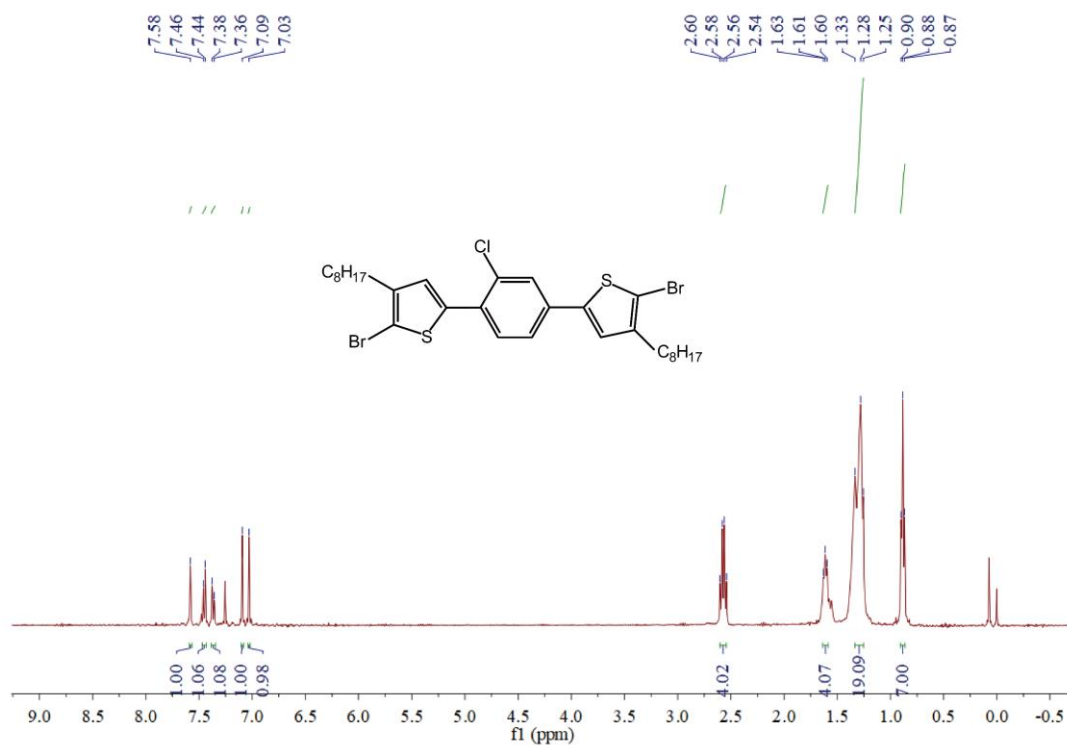
Fig. S30. ¹H NMR spectrum of the Br-T-1ClB-T-Br. Chemical shifts were recorded in delta (δ) units, expressed in parts per million (ppm). Protonated $CDCl_3$ was used as the solvent for recording ¹H (of residual proton; $CDCl_3$, δ = 7.26 ppm). The splitting patterns of ¹H NMR have been described as "m, multiple". 1H NMR (400 MHz, $CDCl_3$): δ = 7.58 (s, 1H), 7.45 (d, J = 8.1 Hz, 1H), 7.37 (d, J = 8.1 Hz, 1H), 7.09 (s, 1H), 7.03 (s, 1H), 2.57 (dd, J = 15.7, 8.2 Hz, 5H), 1.65-1.58 (m, 5H), 1.25-1.33 (m, 24H), 0.87-0.90 (m, 8H).

Table S1. Electronic energies and correction to Gibbs free energy of related compounds.

Samples	Electronic energies (eV)	Correction to Gibbs free energy (eV)
P1Cl-T	-442.9999078	12.261044
H@P1Cl-T	-444.4007105	12.414674
g-C$_3$N$_4$	-236.5550813	3.825788
H@g-C$_3$N$_4$	-240.4399978	4.033444
g-C$_3$N$_4$/P1Cl-T	-1395.973053	27.19604
H@g-C$_3$N$_4$/P1Cl-T	-1399.740944	27.466897

Table S2. Parameters for TA kinetics probed at 510 nm for P1Cl-T and 400 nm for g-C_3N_4, and g-C_3N_4/P1Cl-T_7 under the excitation of 365 nm. Solvent: Chloroform.

Sample	τ_1(ps)	A_1 (%)	τ_2(ps)	A_2 (%)	τ_{ave} (ps)
g-C_3N_4	20.18	64.17	755.32	35.83	721.75
g-C_3N_4/P1Cl-T_7	8.48	65.12	358.89	34.88	344.09
P1Cl-T	8.07	45.85	227.43	54.15	221.03

The average lifetime (τ_{ave}) is determined by using the equation as follows[15]:

$$\tau_{ave} = \frac{\sum A_i \tau_i^2}{\sum A_i \tau_i} = (A_1\tau_1^2 + A_2\tau_2^2)/(A_1\tau_1 + A_2\tau_2)\cdots\cdots\cdots\cdots Eq.(3)$$

where A_i refers to the pre-exponential factors and τ_i represents the obtained lifetimes from the bi-exponential fitting of the decay kinetics.

Table S3. The apparent quantum yields (AQYs) of g-C$_3$N$_4$/P1Cl-T$_7$ heterojunction at various wavelengths.

Wavelength (nm)	Light intensity (mW cm^{-2})	Area (cm^2)	Amount of H$_2$ (μmol)	AQY (%)
475	8	0.25	6.68	46.75
520	8	0.25	6.18	39.50
600	6	0.25	0.34	2.51
700	18	0.25	0.84	1.77

λ = 475 nm:

$$N = \frac{E\lambda}{hc} = \frac{8\times10^{-3}\times0.25\times3600\times475\times10^{-9}}{6.626\times10^{-34}\times3\times10^{8}} = 1.72 \times 10^{19}$$

$$AQY = \frac{the\ number\ of\ reacted\ electrons}{the\ number\ of\ incident\ photons} \times 100\% = \frac{2\times the\ number\ of\ evolved\ H_2\ molecules}{N} \times 100\% =$$

$$\frac{2\times6.02\times10^{23}\times6.68\times10^{-6}}{1.72\times10^{19}} \times 100\% = 46.75\%$$

λ = 520 nm:

$$N = \frac{E\lambda}{hc} = \frac{8\times10^{-3}\times0.25\times3600\times520\times10^{-9}}{6.626\times10^{-34}\times3\times10^{8}} = 1.88 \times 10^{19}$$

$$AQY = \frac{the\ number\ of\ reacted\ electrons}{the\ number\ of\ incident\ photons} \times 100\% = \frac{2\times the\ number\ of\ evolved\ H_2\ molecules}{N} \times 100\% =$$

$$\frac{2\times6.02\times10^{23}\times6.18\times10^{-6}}{1.88\times10^{19}} \times 100\% = 39.50\%$$

λ = 600 nm:

$$N = \frac{E\lambda}{hc} = \frac{6\times10^{-3}\times0.25\times3600\times600\times10^{-9}}{6.626\times10^{-34}\times3\times10^{8}} = 1.63 \times 10^{19}$$

$$AQY = \frac{the\ number\ of\ reacted\ electrons}{the\ number\ of\ incident\ photons} \times 100\% = \frac{2\times the\ number\ of\ evolved\ H_2\ molecules}{N} \times 100\% =$$

$$\frac{2\times6.02\times10^{23}\times0.34\times10^{-6}}{1.63\times10^{19}} \times 100\% = 2.51\%$$

λ = 700 nm:

$$N = \frac{E\lambda}{hc} = \frac{18\times10^{-3}\times0.25\times3600\times700\times10^{-9}}{6.626\times10^{-34}\times3\times10^{8}} = 5.70 \times 10^{19}$$

$$AQY = \frac{the\ number\ of\ reacted\ electrons}{the\ number\ of\ incident\ photons} \times 100\% = \frac{2\times the\ number\ of\ evolved\ H_2\ molecules}{N} \times 100\% =$$

$$\frac{2\times6.02\times10^{23}\times0.84\times10^{-6}}{5.70\times10^{19}} \times 100\% = 1.77\%$$

Table S4. Comparison of photocatalytic performance of g-C$_3$N$_4$/P1Cl-T with other organic-based photocatalysts. "-" means unknown data.

Photocatalysts	absorption edge (nm)	Co-catalyst	Light source	Temperature (°C)	HER (mmol·h^{-1}·g^{-1})	AQY	Ref.
g-C$_3$N$_4$/P1Cl-T	750	3 wt% Pt	≥420 nm	15	111.8	46.7%@475 & 1.77%@700 nm	This work
PCN/TBT	600	3 wt% Pt	780≥λ≥420 nm	25	20.1	3.0%@450 nm & 0.3%@550 nm	16
P3/CN	700	1 wt% Pt	780≥λ≥420 nm	-	13.0	27.3%@520 nm & 0.6%@700 nm	17
Pt–P@CN	600	0.24 wt% Pt	AM 1.5 solar simulator	-	2.452	1.43%@420 nm	18
g-PAN/g-C$_3$N$_4$	500	1.5 wt% Pt	≥420 nm	-	0.037	-	19
g-C$_3$N$_4$/P3HT	-	1 wt% Pt	-	-	4.018	2.9%@420 nm	20
PCzF/g-C$_3$N$_4$	550	1 wt% Pt	≥420 nm	35	0.628	27%@440 nm	21
PFBT/g-C$_3$N$_4$	650	1 wt% Pt	≥420 nm	35	0.7223	13%@500nm	21
PEDOT/g-C$_3$N$_4$	-	2 wt% Pt	≥400	-	0.33	-	22
CTF-BT/Th-1	550	10 wt% Pt	≥420 nm	25	6.6	7.3%@420 nm	23
PTB7-Th/EH-IDTBR	800	3 wt% Pt	800≥λ≥350 nm	-	60	2.0%@400 nm & 6.2%@700 nm	24
PIFDTBT Pdots/CNNS	750	-	≥400 nm	Room temperature	0.578	3.4%@420 nm	25
P-COF-1/CTF	550	3 wt% Pt	≥420 nm	6	14.1	-	26
HMP-3_2:3	625	5 wt% Pt	≥395 nm	-	1.6	-	27
P–COF-1/PCN	425	3 wt% Pt	≥420 nm	-	1.105	1.2 %@420 nm & 0.37%@500 nm	28
PFBT/PFODTBT/ITIC	775	6 wt% Pt	>420 nm	-	60.8	2.2 %@450 nm & 4.1%@700 nm	29
TPPS/C$_{60}$	850	6 wt% Pt	Full spectrum	-	34.57	1.22 %@450 nm & 0.1%@700 nm	30
GQDs/PDI	460	3wt% Pt	>420 nm	5	1.6	0.5 %@420 nm & 1.04%@500 nm	31
GD-C$_3$N$_4$	750	3wt% Pt	≥420 nm	12	23.06	31.1% at 420 nm & 2%@600 nm	32
CN/FeNiP/g-C$_3$N$_4$	600	-	≥420 nm	-	13.81	45.8%@420nm	33
BP/CN	1700	-	≥420 nm	-	0.429	3.2% at 420 nm & 1.1%@700 nm	34
CN-acetone	650	2 wt% Pt	≥420 nm	-	29.33	26.2%@400 nm & 0.3%@610 nm	35
Nb$_2$O$_5$/2D g-C$_3$N$_4$	500	3 wt% Pt	≥420 nm	10	12.6	50.6%@405 nm & 0.87%@450 nm	36
SA-Pt/g-C$_3$N$_4$	475	8.7 wt% Pt	≥420 nm	10	22.65	22.5%@420nm	37
CMP/graphene	750	3 wt% Pt	>420 nm	-	0.977	0.36 %@420 nm & 0.05%@600 nm	38
ZnTCPP/THPP	941	6 wt% Pt	≥420 nm	5	41.4	31.7 %@420 nm & 1.3%@650 nm	14

References

1. S. Park, W. J. Chang, C. W. Lee, S. Park, H. Y. Ahn and K. T. Nam, *Nat. Energy*, 2017, **2**, 16185.

2. J. Pommerehne, H. Vestweber, W. Guss, R. F. Mahrt, H. Bässler, M. Porsch and J. Daub, *Adv. Mater.*, 1995, **7**, 551-554.

3. H. Li, H. Yu, X. Quan, S. Chen and Y. Zhang, *ACS Appl. Mater. Interfaces*, 2016, **8,** 2111-2119.

4. G. Kresse and J. Furthmiiller, *Comput. Mater. Sci.*, 1996, **6**, 15-50.

5. G. Kresse, *Phys. Rev. B*, 1996, **54**, 11169-11186.

6. J. P. Perdew, K. Burke and M. Ernzerhof, *Phys. Rev. Lett.*, 1996, **77**, 3865-3868.

7. G. Stefan, A. Jens, E. Stephan and K. Helge, *J. Chem. Phys.* 2010, **132**, 154104.

8. H. J. Monkhorst and J. D. Pack, *Phys. Rev.* B, 1976, **13**, 5188-5192.

9. M. Frisch，G. Trucks，H. Schlegel，G. Scuseria，M. Robb，J. Cheeseman，G. Scalmani，V. Barone，B. Mennucci and G. Petersson, Gaussian 09, revision D.01; Gaussian, Inc.: Wallingford, CT, 2013.

10. A. D. Becke, *J. Chem. Phys.*, 1993, **98**, 5648.

11. C. Lee, W. Yang and R. G. Parr, *Phys. Rev. B*, 1988, **37**, 785.

12. E. Gao, W. Wang, M. Shang and J. Xu, *Chem. Chem. Phys.*, 2011, **13,** 2887-2893.

13. T. Simon, N. Bouchonville, M. J. Berr, A. Vaneski, A. Adrović, D. Volbers, R. Wyrwich, M. Döblinger, A. S. Susha, A. L. Rogach, F. Jäckel, J. K. Stolarczyk and J. Feldmann, *Nat. Mater.*, 2014, **13,** 1013–1018.

14. J. Jing, J. Yang, W. Li, Z. Wu and Y. Zhu, *Adv. Mater.*, 2021, **34**, 2106807.

15. Z. Zhang, Y. Huang, K. Liu, L. Guo, Q. Yuan and B. Dong, *Adv. Mater.*, 2015, **27,** 5906-5914.

16. K. Li, L. Wang, Z. Chen, X. Yang, Y. Yu, W. Zhang, Y. Wang, Y. Shi, K. P. Loh and Q. Xu, *Adv. Funct. Mater.*, 2020, **30**, 2005106.

17. F. Yu, Z. Wang, S. Zhang, H. Ye, K. Kong, X. Gong, J. Hua and H. Tian, *Adv. Funct. Mater.*, 2018, **28,** 1804512.

18. X. Zhou, Y. Liu, Z. Jin, M. Huang, F. Zhou, J. Song, J. Qu, Y. Zeng, P. Qian, W. Wong, *Adv. Sci.*, 2021, **8**, 2002465.

19. F. He, G. Chen, Y. Yu, S. Hao, Y. Zhou and Y. Zheng, *ACS Appl. Mater. Interfaces*, 2014, **6,** 7171-7179.

20. H. Yan and Y. Huang, *Chem. Commun.*, 2011, **47,** 4168-4170.

21. J. Chen, C. Dong, D. Zhao, Y. Huang, X. Wang, L. Samad, L. Dang, M. Shearer, S. Shen and L. Guo, *Adv. Mater.,* 2017, **29,** 1606198.

22. Z. Xing, Z. Chen, X. Zong and L. Wang, *Chem. Commun.*, 2014, **50,** 6762-6764.

23. W. Huang, Q. He, Y. P. Hu and Y. G. Li, *Angew. Chem.,* 2019, **131**, 8768-8772.

24. J. Kosco, M. Bidwell, H. Cha, T. Martin, C.T. Howells, M. Sachs, D.H. Anjum, S. Gonzalez Lopez, L. Zou, A. Wadsworth, W. Zhang, L. Zhang, J. Tellam, R. Sougrat, F. Laquai, D.M. Delongchamp, J.R. Durrant and I. Mcculloch, *Nat. Mater.*, 2020, **19,** 559-565.

25. W. Zhou, T. Jia, D. Q. Zhang, Z. K. Zheng, W. Hong and X. D. Chen, *Appl. Catal. B Environ.*, 2019, **259**, 118067.

26. N. Xu, Y. Liu, W. Yang, J. Tang, B. Cai, Q. Li, J. Sun, K. Wang, B. Xu, Q. Zhang and Y. Fan, *ACS Appl. Energy Mater.*, 2020, **3**, 11939-11946.

27. K. Kailasam, M. B. Mesch, L. Möhlmann, M. Baar, S. Blechert, M. Schwarze, M. Schröder, R. Schomäcker, J. Senker and A. Thomas, *Energy Technol.,* 2016, **4,** 744-750.

28. J. Tang, Q. Li, Y. Liu, N. Xu, K. Wang, Q. Zhang, W. Yang and Y. Fang, *Int. J. Hyd. Energy*, 2021, **46**, 17666-17676.

29. A. Liu, L. Gedda, M. Axelsson, M. Pavliuk, K. Edwards, L. Hammarström and H. Tian, *J. Am. Chem. Soc.*, 2021, **143,** 2875-2885.

30. J. Yang, J. F. Jing and Y. F. Zhu, *Adv. Mater.*, 2021, **33**, 2101026.

31. J. Yang, H. Miao, J. F. Jing, Y. F. Zhu and W. Y. Choi, *Appl. Catal. B Environ.*, 2021, **281**, 119547.

32. Y. Yu, W. Yan, X. Wang, P. Li, W. Gao, H. Zou, S. Wu and K. Ding, *Adv. Mater.,* 2018, **30,** 1705060.

33. J. Xu, Y. Qi, C. Wang and L. Wang, *Appl. Catal. B Environ.*, 2019, **241,** 178-186.

34. M. Zhu, S. Kim, L. Mao, M. Fujitsuka, J. Zhang, X. Wang and T. Majima, *J. Am. Chem. Soc.*, 2017, **139,** 13234-13242.

35. L. Jiang, J. Li, K. Wang, G. Zhang, Y. Li and X. Wu, *Appl. Catal. B Environ.*, 2020, **260,** 118181.

36. J. Yi, T. Fei, L. Li, Q. Yu, S. Zhang, Y. Song, J. Lian, X. Zhu, J. Deng, H. Xu and H. Li, *Appl. Catal. B Environ.*, 2021, **281,** 119475.

37. Z. Zeng, Y. Su, X. Quan, W. Choi, G. Zhang, N. Liu, B. Kim, S. Chen, H. Yu and S. Zhang, *Nano Energy*, 2020, **69,** 104409.

38. Z. F. Qian, Y. J. Yan, Z. Q. Liang, X. D. Zhuang and K. A. I. Zhang, *Mater. Adv.,* 2021, **2**, 7379-7383.